Molecular Therapy
Oncology
Brief report

Longitudinal tracking of *MALAT1* level over a breast cancer patient's course of treatment and disease progression

Disha Aggarwal,[1,2] Tse-Luen Wee,[1] Shuchismita Satpathy,[1,3] Suzanne Russo,[1] and David L. Spector[1,2]

[1]Cold Spring Harbor Laboratory, Cold Spring Harbor, NY 11724, USA; [2]Genetics Graduate Program, Stony Brook University, Stony Brook, NY 11794, USA; [3]Division of Medical Oncology/Hematology, Northwell Health, New Hyde Park, New York 11042, USA

Long non-coding RNAs (lncRNAs) have emerged as important regulators of the hallmarks of cancer, yet their potential remains under-explored in clinical studies. *Metastasis-Associated Lung Adenocarcinoma Transcript 1* (*MALAT1*), an lncRNA upregulated in over 20 tumor types including breast tumors, has been associated with metastasis, yet its expression across the clinical course of treatment and disease progression remains uncharacterized. For the first time, this case report evaluated *MALAT1* level in multiple biopsies collected over a breast cancer patient's clinical course of treatment spanning 2.5 years, using quantitative single-molecule RNA fluorescence *in situ* hybridization. We observed that *MALAT1* levels were consistently elevated in tumor cells relative to adjacent stroma, reduced upon standard-of-care therapeutic interventions, and markedly increased in distant metastatic lesions. These longitudinal changes in expression level demonstrate a link between *MALAT1* and disease progression. Our findings highlight the potential of *MALAT1* as a prognostic marker for treatment response and metastatic risk stratification and support pursuing *MALAT1* as a therapeutic target.

INTRODUCTION

Breast cancer (BC) remains one of the most prevalent malignancies in women worldwide with a high level of patient heterogeneity.[1,2] Although advances in early detection and targeted therapies have improved patient outcomes, metastasis and recurrence remain the major clinical challenges responsible for the majority of BC-related deaths.[3] Metastasis and recurrence are often driven by residual cancer cells that manage to undergo molecular/genetic changes to become dormant and/or undergo immune evasion to survive primary treatments.[4–6] These cells re-emerge from dormancy years later leading to recurrence and distant metastasis.

Long non-coding RNAs (lncRNAs) have gained considerable attention in recent years for their regulatory roles in gene expression.[7] Among them, *Metastasis-Associated Lung Adenocarcinoma Transcript 1* (*MALAT1*) is one of the most highly studied lncRNAs in normal biology as well as in disease contexts.[8] *MALAT1* was first identified in a microarray screen where it was found to be overexpressed in early-stage lung tumors that later metastasized in patients.[9] Since then, it has been implicated for its oncogenic role in over 20 cancer types and has been linked to tumor proliferation, metastasis, and therapy resistance.[8,10] *MALAT1* is known to be localized primarily to nuclear speckles, structures that are enriched in factors involved in various steps in RNA processing.[11–13]

MALAT1 has been shown to be upregulated in human breast tumors when compared to normal breast tissues by quantitative reverse-transcription PCR (RT-qPCR).[14–17] A comparison of *MALAT1* expression in different subtypes of BC patients in The Cancer Genome Atlas (TCGA) database and RT-qPCR analysis of other patient cohorts showed that hormone receptor-positive tumors (i.e. ER(+), estrogen receptor-positive and PR(+), progesterone receptor-positive) have higher *MALAT1* levels than triple-negative breast cancer (TNBC) or ER(−), PR(−), and HER2(+), human epidermal growth factor receptor 2-positive patients.[18,19] Further, two datasets of tamoxifen-treated ER(+) BC patients showed decreased recurrence-free survival (RFS) in high-*MALAT1*-expressing patients.[14] Additionally, studies have shown that high *MALAT1* expression correlates with worse RFS in ER(−) negative BC patients.[14,19,20] In lymph node-negative TNBC patients, elevated *MALAT1* expression has also been shown to be associated with worse disease-specific survival, indicating strong prognostic significance.[18] Disease-specific survival estimations exclude death from other causes while accounting only for death caused by the disease itself—unlike disease-free survival. High *MALAT1* expression was also shown to be associated with worse overall survival in all BCs in TCGA database.[21]

While the bulk of studies on *MALAT1* has strongly implicated its oncogenic role[10,22] (and as discussed earlier), three studies have suggested a tumor-suppressive role in BC.[23–25] While Kim et al.[24] have suggested that previously reported changes in expression of adjacent genes in the *Malat1* knockout (KO) mouse[26] to be responsible for the oncogenic phenotype, they fail to point out that those gene

Received 1 August 2025; accepted 15 October 2025;
https://doi.org/10.1016/j.omton.2025.201070.

Correspondence: David L. Spector, Cold Spring Harbor Laboratory, Cold Spring Harbor, NY 11724, USA.
E-mail: spector@cshl.edu

expression changes were originally reported for the brain cortex.[26] Recently, we have analyzed RNA expression in the mammary glands of these KO mice, and we do not observe any significant changes in the expression of *Malat1*-adjacent genes (Aggarwal, D., Russo, S. and Spector, D.L., unpublished data).

Despite growing interest in the lncRNA *MALAT1* as a therapeutic target,[10,21,27–31] there remains a dearth of data on how its expression pattern evolves longitudinally over the course of treatment and disease progression in patients. Several bulk RNA sequencing or RT-qPCR studies have previously evaluated *MALAT1* expression levels in primary breast tumors.[14,15,17,18,32] However, these bulk transcriptomic approaches lack the spatial resolution necessary to capture the subcellular localization as well as cell-to-cell heterogeneity in expression across a tumor tissue vs. the adjacent stromal cells. Single-molecule RNA fluorescence *in situ* hybridization (smRNA-FISH) overcomes these limitations by using a sequence-specific set of probes that directly bind to the intact RNA target in fixed tissue sections. The binding of probes is followed by amplification of the signal via the hybridization chain reaction (HCR).[33] The fluorescence signal was captured using the Zeiss LSM980 Airyscan2 laser scanning confocal microscope, and intensity was quantified using the Imaris image analysis software. This high-resolution microscopy data enable direct visualization of overall expression intensity as well as sub-cellular localization at the single-cell level. This makes smRNA-FISH an ideal method for profiling transcripts, particularly lncRNAs that often show cell-type-specific expression and distinct subcellular distribution patterns.[7]

In this case report, we employ smRNA-FISH to evaluate the expression level and spatial distribution of *MALAT1* longitudinally across multiple stages of clinical treatment in samples from a BC patient, spanning a 2.5-year period. By analyzing biopsy samples collected at key clinical milestones—including primary diagnosis, post-treatment relapse, and metastatic progression—we found that *MALAT1* levels evolve in response to treatment and disease progression. *MALAT1* level was high in the treatment-naive primary tumor and reduced in the biopsy samples after chemotherapy and immunotherapy but were the highest in the distant metastatic lesion. Further, *MALAT1* level in cells from the tumors and metastatic lesions was always higher than that in cells in the adjacent stromal compartment.

RESULTS

Case presentation

A 59-year-old white female with unknown past medical and family history initially presented after palpating a lump in her right breast. A diagnostic mammogram of the right breast showed a 1 cm tumor at 10:00 o' clock position, 6 cm from the nipple, likely malignant in nature (Figure 1). An ultrasound of the right breast revealed the tumor to be 0.3 × 1.4 cm. Right axilla ultrasound indicated a suspicion of lymph node involvement as well. An ultrasound-guided core needle biopsy (biopsy #1) of the tumor identified it to be grade 3 invasive ductal carcinoma. The molecular pathology of the tumor was ER negative (<1%), PR weakly positive (9%), and Her2 negative (0%), consistent with clinical TNBC. No lympho-vascular invasion was observed. Furthermore, biopsy of the right axilla did not confirm any lymph node involvement. Her disease was diagnosed as clinical stage T1cNxM0 TNBC. The patient was then given the standard first-line neoadjuvant therapy of dose-dense AC-T (doxorubicin and cyclophosphamide followed by paclitaxel) for 5 months. The patient then underwent lumpectomy to remove the tumor 7 months after her initial diagnosis, followed by 2 months of radiation therapy post-lumpectomy. Given pathology results from the lumpectomy showed residual disease in the breast, she was started on capecitabine (Xeloda) treatment. After continuing full dose of Xeloda for 2 months, the patient had severe side effects to Xeloda. Hence, Xeloda was held for 2 months and then eventually restarted with 50% dose reduction, which she continued for the next 5 months. A month later, the patient presented with two suspicious lesions in the same breast concerning for BC recurrence. Two core needle biopsies were performed. The first one was at least a 5 mm lesion at 10:00 o' clock position, 3 cm from the nipple with pathology consistent with triple-negative subtype (biopsy #2). The second one was a 6 mm lesion at 10:00 o' clock position, 7 cm from the nipple, and was ER(+ at 39%), PR(− but very weak), and Her2(−) upon histopathological analysis (biopsy #3). Both were classified as grade 3, without lympho-vascular invasion. Two months later, the patient underwent bilateral mastectomy for recurrent invasive ductal carcinoma. However, the surgical margins were not clear. The patient then received combinatorial chemotherapy and immunotherapy for 4 months with carboplatin, gemcitabine, and pembrolizumab (Keytruda). Two months after completion of chemotherapy, she presented with skin nodules in the mastectomy flap of the right chest wall, concerning for dermal metastatic disease. Thus, skin punch biopsies were performed at 9:00 and 12:00 positions, and both were identified to be TNBC (biopsy #4). The patient received proton beam therapy to the right chest wall for 3 months. However, post-radiation treatment, the patient presented with a rash to the left chest wall concerning for contralateral chest wall metastasis. Histopathological analysis of the skin punch biopsy (biopsy #5) of left chest wall revealed grade 3 TNBC metastatic disease involving the dermal soft tissue and lymphatic spaces. The patient eventually succumbed to metastatic TNBC after three and a half years since her initial cancer diagnosis.

Tumor/metastatic lesions have higher *MALAT1* levels compared to adjacent stroma, as visualized by single-molecule RNA fluorescence *in situ* hybridization

Previous studies using "bulk" approaches such as RT-qPCR or RNA sequencing have shown that *MALAT1* is upregulated in breast tumors compared to matched normal breast tissues (Shao et al.[15]; Yue et al.[16]). In three paired patient breast tumor and metastasis-derived tissues, our laboratory has previously reported visibly elevated *MALAT1* level in cancer cells compared to adjacent stroma using RNA-FISH.[34] Here, we performed single-molecule RNA-FISH to directly compare and quantify *MALAT1* expression in the tumor and stromal areas of the procured patient's BC biopsy tissues over the course of treatment and tumor progression. Using the HCR v.3.0 technology with split-initiator probes,[35] we successfully observed *MALAT1* expression via smRNA-FISH with a high signal-to-background ratio and robust reproducibility. Tumor and stromal areas were identified using

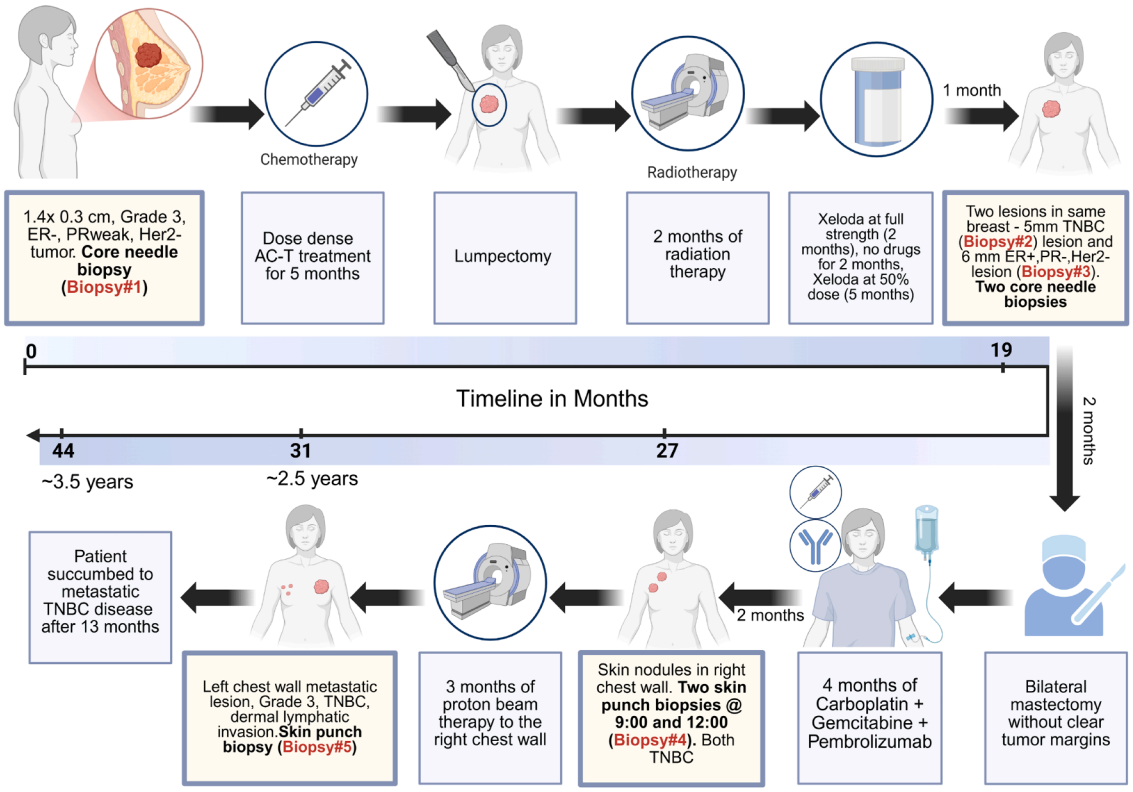

Figure 1. Schematic representation of the patient case history

Detailed schematic of the patient's course of breast cancer progression over 2.5 years. The 5 biopsy samples analyzed in this project are highlighted in red text. TNBC, triple-negative breast cancer; AC-T, doxorubicin (A), cyclophosphamide (C), and paclitaxel (T); ER, estrogen receptor; PR, progesterone receptor; Her2, human epidermal growth factor receptor 2. Created in BioRender. Aggarwal, D. (2025) https://BioRender.com/qrbl2sf.

hematoxylin and eosin (H&E) staining on formalin-fixed, paraffin-embedded (FFPE) 5 μm tissue sections (Figures 2A and 2I). The adjacent serial section was used for smRNA-FISH to allow clear demarcation of stromal and tumor regions. DAPI staining was utilized to identify cell nuclei. For each tumor/metastasis biopsy tissue block, we performed smRNA-FISH and imaging on two sections that were 40 μm apart within the tissue blocks. We observed *MALAT1* to be exclusively localized to the nuclei in all samples, consistent with previously published studies on *MALAT1*.[11–13] Furthermore, comparison of the treatment-naive breast tumor and surrounding stroma clearly showed significantly higher *MALAT1* expression in tumor cells compared to the normal cell types in the stroma (Figures 2B–2D). This trend was observed in all biopsy samples, including the contralateral breast metastasis biopsy (Figures 2E and 2I) where the metastatic lesion has significantly higher *MALAT1* expression compared to the surrounding stroma (Figures 2E–2L).

smRNA-FISH reveals the longitudinal modulation in *MALAT1* levels across the patient's course of treatment and disease progression

To assess the dynamics of *MALAT1* expression over the period of the patient's disease progression and intervening treatments, we examined the *MALAT1* smRNA-FISH intensity specifically in the tumor areas of biopsy tissues taken at different time points. Each biopsy block had 1–3 pieces of tissue that were imaged using the Zeiss LSM980 Airyscan2 laser scanning confocal microscope following smRNA-FISH. Figures 3A–3D present representative areas from tissue sections. The treatment-naive tumor tissue from biopsy #1 (naive tumor sample in Figure 1) showed high *MALAT1* expression (Figure 3A). After lumpectomy, radiation therapy, and chemotherapy, the patient relapsed with two tumors—one TNBC (biopsy #2 in Figure 1) and the other ER positive (biopsy #3 in Figure 1). *MALAT1* expression decreased in both tumors compared to the initial treatment-naive tumor, and the representative image from the TNBC tumor is shown in Figure 3B. After bilateral mastectomy and additional adjuvant chemotherapy in combination with immunotherapy for recurrent disease, the patient then developed local skin metastases in the right chest wall (biopsy #4 in Figure 1), which also exhibited lower *MALAT1* expression (Figure 3C). The patient subsequently underwent proton beam therapy to the right chest wall for 3 months but later presented with a rash in the left chest area. *MALAT1* expression was markedly higher in the contralateral (left chest wall) breast tumor metastasis biopsy tissue (biopsy #5 in Figure 1) than in the earlier biopsy samples (Figure 3D).

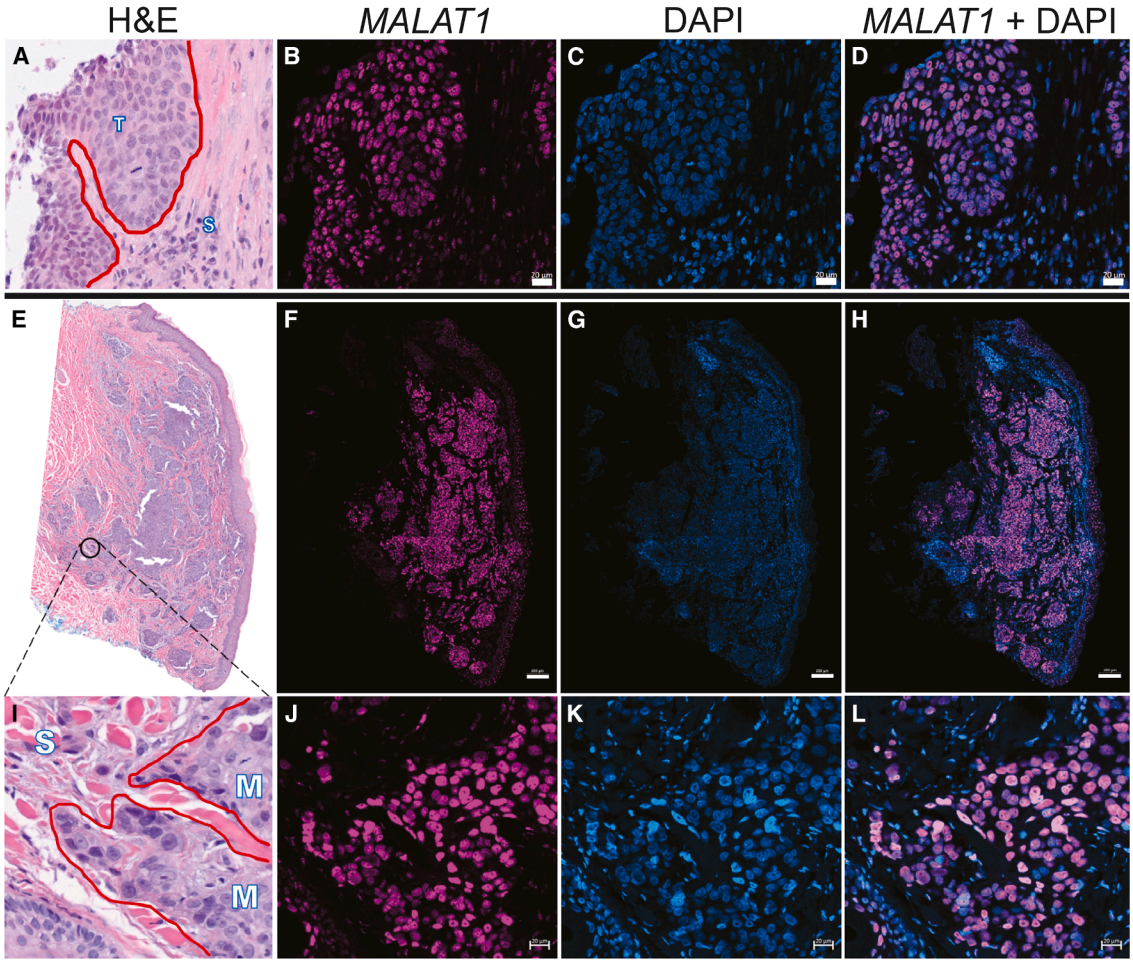

Figure 2. *MALAT1* expression in patient stromal tissue and tumor/metastatic lesions via smRNA-FISH

Representative image of smRNA-FISH using *MALAT1*-targeting probes on the patient's naive tumor biopsy. (A) Hematoxylin and eosin staining revealing tumor area (T) and the adjacent stroma (S). (B) smRNA-FISH performed on the adjacent serial section displaying *MALAT1* FISH signal in pink. (C) Single-channel image showing corresponding nuclear DAPI signal (blue). (D) Corresponding merged image. (E) Hematoxylin and eosin (H&E) staining of a tissue region in the contralateral breast metastasis biopsy sample. (F) smRNA-FISH for *MALAT1* on adjacent serial section (pink, *MALAT1* signal). (G) DAPI channel (blue). (H) Merged channels. (I) Inset of a zoomed-in area of H&E-stained metastasis section (labeled M). Areas surrounded by red line represent metastatic regions, and normal stromal region is labeled S (J) *MALAT1* channel. (K) DAPI channel. (L) Corresponding merged image. *MALAT1* RNA transcripts in pink, DAPI nuclear staining in blue. Scale bar for (E)–(H) = 200 μm; scale bar for (A)–(D) and (I)–(L) = 20 μm.

Fluorescence intensity was quantified using Imaris software, analyzing 3–5 regions of interest per slide. Cumulatively, data from approximately 1,200 nuclei per biopsy sample (∼600 nuclei in each section) were collated. For each biopsy tissue, we consistently observed higher *MALAT1* expression in the tumor/metastasis regions (labeled T/M) compared to the adjacent stroma (labeled S), as identified by H&E staining (Figure 3E). This difference was found to be statistically significant, as assessed by Wilcoxon rank sum/Mann-Whitney U test.

Additionally, comparing the tumor areas across the different biopsy samples confirms the trend observed visually in Figures 3A–3D. *MALAT1* expression is high in the initial treatment-naive tumor (biopsy #1 in Figure 1) (Figure 3E). After lumpectomy, radiation therapy, and chemotherapy, *MALAT1* expression is reduced in the relapsed tumors. However, the TNBC tumor (biopsy #2 in Figure 1) shows a more pronounced reduction than the ER(+) relapsed tumor (biopsy #3 in Figure 1) (Figure 3E). Following bilateral mastectomy and a combinatorial regimen of chemotherapy and immunotherapy, the metastasized local skin nodules (biopsy #4 in Figure 1) also exhibit low *MALAT1* expression (Figure 3E). Notably, however, the distant skin metastasis in the contralateral (left) chest wall (biopsy #5 in Figure 1) shows a drastic elevation in *MALAT1* expression (Figure 3E). In fact, the *MALAT1* expression in the cells in the contralateral metastasis biopsy tissue is significantly higher ($p = 1.09 \times 10^{-18}$) compared to the already highly expressing cells in the treatment-naive primary tumor. The median values of the violin plots highlight this dynamic trend in *MALAT1* expression

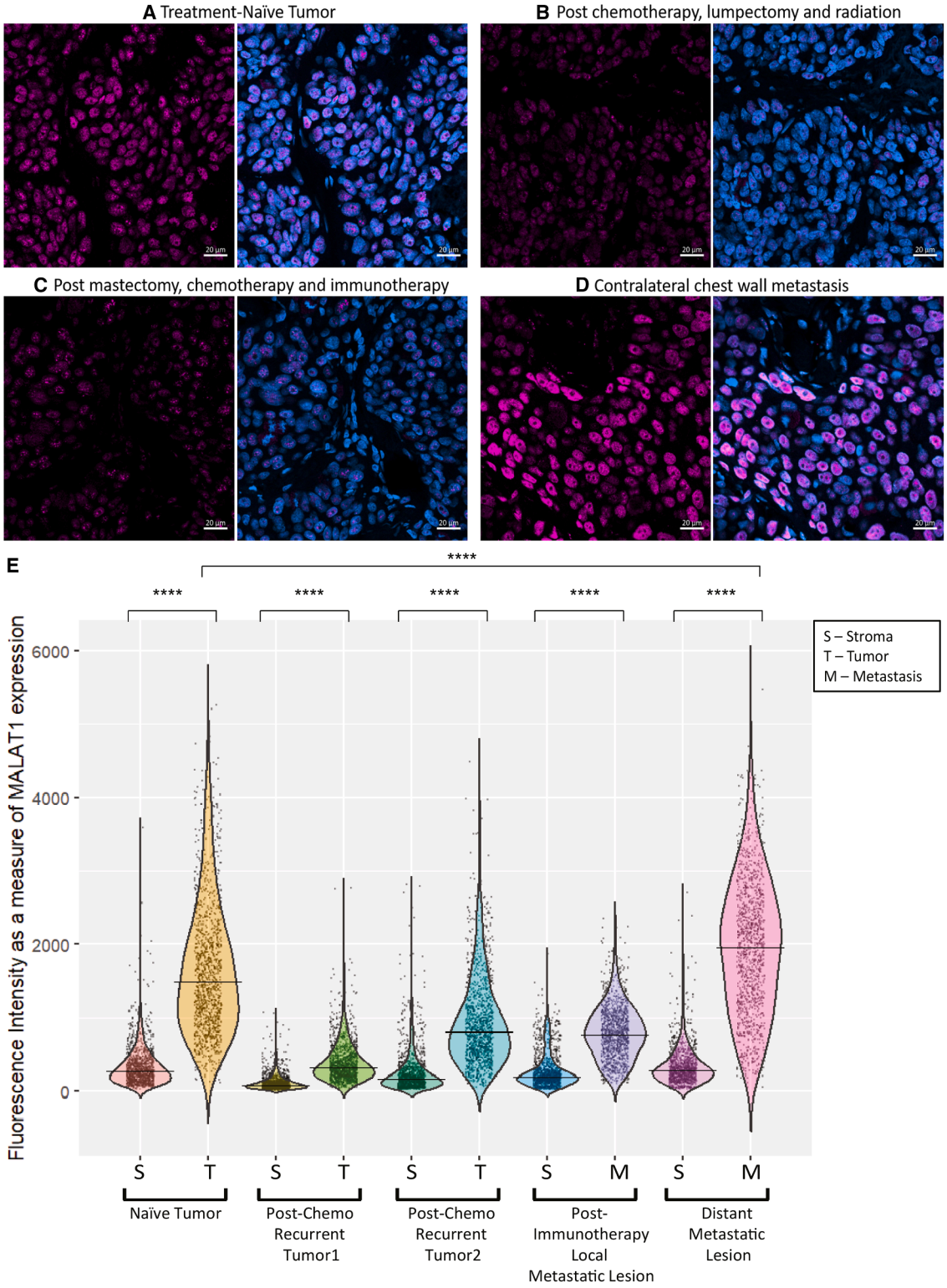

Figure 3. Visualization of *MALAT1* expression longitudinally over disease progression

Representative images showing *MALAT1* expression as visualized using smRNA-FISH on sections of a breast cancer patient's biopsies (tumor/metastasis) from different time points across their treatment regimen and disease progression. (A) Treatment-naive tumor; (B) relapsed TNBC tumor post-lumpectomy, adjuvant chemotherapy, and

(legend continued on next page)

over the course of treatment and disease progression. Since *MALAT1* is known to localize to nuclear speckles within cell nuclei,[11–13] we sought to determine whether the overall increase in *MALAT1* expression leads to a corresponding increase in its speckled distribution. To investigate this, we counted the number of speckles per cell nucleus using Imaris software (Figure S1A). We observed that the samples with high overall *MALAT1* intensity also had the highest number of *MALAT1* speckles per nucleus (Figure S1B). This confirms that, upon increased expression, *MALAT1* subnuclear distribution is concentrated in an increased number of nuclear speckles.

DISCUSSION

This study provides the first in-depth spatial and longitudinal profiling of *MALAT1* expression throughout the clinical course of treatment and disease progression of a BC patient. Consistently, across all time points and respective biopsy samples, *MALAT1* expression in tumor cells was found to be markedly higher compared to the adjacent stromal compartment. The persistent tumor-specific enrichment we observed via smRNA-FISH, both visually and quantitatively, corroborates and extends our previous findings[34] implicating *MALAT1* in BC progression.

Interestingly, a reduction in *MALAT1* level was observed in the two relapsed lesions following chemotherapy and radiation therapy, relative to the original treatment-naive tumor. The consecutive biopsy sample from the relapsed local skin metastasis in the same right chest area, after prolonged chemotherapy and immunotherapy, also showed reduced *MALAT1* expression. This finding was particularly surprising, as metastatic tissues have often been reported to exhibit higher *MALAT1* expression than primary breast tumors.[21,34] However, previous studies have predominantly analyzed metastases in distant organs, which may explain the absence of this trend in the local recurrence biopsy sample. The observed decline in *MALAT1* expression may be reflective of treatment-induced alterations in the tumor cell transcriptome. Careful examination of a large number of patient tumors and metastases, both pre- and post-treatment, is warranted to discern how *MALAT1* transcript levels are modulated in response to cytotoxic and immunomodulatory therapies and whether these changes correlate with patient outcomes. This potential of *MALAT1* as a prognostic marker for assessing treatment response could be highly valuable in the clinic.

Previous work from our lab and others has demonstrated upregulation of *MALAT1* in distant metastatic tissues compared to matched primary breast tumors via RNA-FISH.[21,34] The present work visually demonstrates the spatial distribution of *MALAT1* in patient biopsy tissues across disease and treatment progression and quantifies signal intensity of *MALAT1* at the level of individual nuclei. We observed statistically significant upregulation of *MALAT1* in the distant contralateral breast metastasis, compared to the treatment-naive primary tumor.

High *MALAT1* expression has been shown to significantly correlate with increased metastasis in multiple cancer types.[9,36] Additionally, several studies have shown that *Malat1* depletion in multiple mouse models results in reduced metastasis of breast and lung cancer.[21,34,37,38] Given the findings of these pre-clinical studies, *MALAT1* is an attractive target for metastatic BC. Our findings in conjunction with previous studies suggest that, irrespective of the current standard-of-care treatment, distant metastatic tissues display high levels of *MALAT1* and hence combining a *MALAT1*-targeting antisense oligonucleotide (ASO) therapy with current treatments may alleviate or reduce metastatic disease.

Combining *MALAT1*-targeting ASO with carboplatin or anti-PD1 antibody in syngeneic mouse models of BC showed augmented treatment response by enhancing T cell infiltration of the tumor.[31] In addition, single-cell RNA sequencing comparing TNBC tumors ($n = 3$) from patients who responded to neo-adjuvant chemotherapy versus those with residual disease found that *MALAT1* transcripts were upregulated in the chemotherapy-resistant group, suggesting a link between *MALAT1* and chemoresistance.[39] While our study differs in scope and methodology, the observed reduction in *MALAT1* expression in post-treatment relapsed tumors, followed by a drastic increase in *MALAT1* levels in the distant contralateral metastatic sample, supports this proposed link between *MALAT1* and chemoresistance. Moreover, Kumar et al. have identified *Malat1* as a critical regulator of dormancy in BC.[21] They show that *Malat1* is required to facilitate the metastatic reactivation of quiescent breast tumor cells by aiding them in evading immune surveillance. Abrogating *Malat1* expression drastically reduces metastatic reactivation of these persister incipient tumor cells.[21] Cumulatively, these insights make a compelling case for therapeutically targeting *MALAT1* in combination with chemotherapy and immunotherapy to prevent outgrowth of these persister cells and thus future metastasis.

Beyond the reported findings, this case study highlights the broader utility of smRNA-FISH in capturing spatially resolved expression patterns of potential biomarkers at single-cell resolution and directly being able to compare tumor vs. stroma *in situ*. The labeling technique and analysis pipeline used here demonstrated robust reproducibility across tissue sections, experimental replicates, and personnel, underscoring the methodological rigor of this approach. This strategy offers a unique opportunity to investigate potential prognostic biomarkers and understand how their expression is

radiation therapy; (C) skin metastasis biopsy post-bilateral mastectomy, chemotherapy, and immunotherapy; (D) contralateral chest wall metastasis. *MALAT1* RNA transcripts in pink, DAPI nuclear staining in blue. Each treatment point shows an image of the *MALAT1* channel on the left and corresponding image with both channels merged (*MALAT1* + DAPI) on the right. Scale bars, 20 μm. (E) *MALAT1* expression as measured by smRNA-FISH and quantified using Imaris software. Each dot represents one cell ($n = \sim$1,200) from quantifying multiple regions from two tissue sections 40 μm apart ($n = \sim$600 each). Horizontal line on each violin plot represents the median value. *p* value calculated using Wilcoxon rank sum/Mann-Whitney U test in R (****p value < 0.0001). S, stroma; T, tumor; and M, metastatic lesion.

dynamically regulated by clinical interventions or longitudinally with disease progression.

In summary, this study provides new insights into the dynamic regulation of *MALAT1* in response to disease progression and standard-of-care therapies for BC. We observed that a *MALAT1*-high primary tumor (ER(−), PR(weak), Her2(−)) relapsed with lower *MALAT1* expression post-chemotherapy (two lesions; TNBC and ER(+), PR(−), Her2(−)). The second recurrence after further disease intervention with additional chemotherapy and immunotherapy presented as a local metastatic lesion (TNBC), exhibiting the same relatively lower *MALAT1* level. However, the subsequent distant metastatic lesion (TNBC) exhibited the highest *MALAT1* level compared to all previous lesions, thus lending support to previous work[21] implicating *Malat1* in the reactivation of incipient metastatic cells in BC. In conclusion, *MALAT1* level is highly dynamic through the course of disease progression/treatment and is likely strongly impacted by disease interventions, irrespective of the hormone receptor status. Further building on this study by physicians and researchers working on similar cases could be beneficial in elaborating on the potential of *MALAT1* expression as a risk factor for stratification to identify patients at higher risk of treatment resistance and distant metastasis.

In addition, these findings advocate for the development of a *MALAT1*-targeting therapy that could potentially target existing metastases and escaper dormant cells and thereby suppress additional metastasis. Notably, a *MALAT1*-targeting ASO is likely to go into clinical trials in the near future. Additional studies across larger patient cohorts will be essential to corroborate the observations presented here and to contribute to determining the optimum timing of administering a *MALAT1*-targeting antisense therapy.

MATERIALS AND METHODS

smRNA-FISH

FFPE patient tissue sections were deparaffinized using xylene, rehydrated using a degrading ethanol gradient, and then treated with heat denaturation in 1× Tris-EDTA antigen retrieval buffer (Abcam ab93684). Then the tissue sections were subjected to proteinase K digestion (Viagen Biotech 501-PK). The Molecular Instruments HCR v.3.0 RNA-FISH assay kit for FFPE tissues[35] was utilized for performing smRNA-FISH. *In situ* HCR v.3.0 uses split-initiator probes that allow direct amplification after target detection thus reducing the process to two steps unlike previous versions of this technology. HCR v.3.0 also displays significantly enhanced specificity as it requires two probes to be bound for amplification to occur and further enhancing automatic background suppression. A probe pool targeting *MALAT1* (Lot#RTJ316) was used at 16 nM concentration. The hybridization and signal amplification steps were performed as per the manufacturer's protocol. Hairpins were labeled with the fluorophore with 647 nm excitation wavelength. Nuclei were counter-stained using DAPI (Thermo Fisher Scientific D1306). The tissue sections were mounted on 0.17 mm thick coverslips using the ProLong Gold Antifade mounting medium (Thermo Fisher Scientific, P36930).

Fluorescence *in situ* imaging and data analysis

Microscopy images were acquired in Airyscan SR-4Y multiplexing mode using a Zeiss LSM 980 Airyscan2 inverted confocal laser scanning microscope (Carl Zeiss Microscopy, White Plains, NY), equipped with Plan-Apochromat 20×/0.8 NA air objective lenses. DAPI was excited using a 405 nm diode laser at 0.7% power, while *MALAT1* probe was excited with a 639 nm diode laser at 1.5% power. Emission signals for both DAPI and *MALAT1* signals were collected using a 32-channel gallium arsenide phosphide (GaAsP-PMT) Airyscan detector, operated in frame scanning mode with a pixel dwell time of 0.51 μs. The DAPI channel was collected with a detector gain of 760 V and emission range of 422–477 nm, while the *MALAT1* channel was collected with a gain of 780 V and emission range of 659–735 nm. Airyscan raw images were processed in Zeiss ZEN Blue 3.8.2 software using Fast Airyscan SheppardSum SR-4Y processing with automated 2D Weiner filter (standard strength).

Further 2D processing and quantitative intensity analysis of *MALAT1* signals were conducted using the Imaris Cell Biologist package (10.2.0, Oxford Instruments). This software facilitated cellular visualization, segmentation of *MALAT1*-positive cells, and quantification of both average *MALAT1* expression and the number of *MALAT1* speckles within individual nuclei. Segmentation parameters, including absolute intensity thresholding and seed point diameter for individual nuclei ID, were optimized based on the DAPI channel. *MALAT1*-positive regions were segmented via absolute intensity thresholding based on *MALAT1* smRNA-FISH intensity and compartmentalized based on DAPI-defined nuclear boundaries. The Spot function, combined with background-corrected thresholding in Imaris, was used to quantify the number of *MALAT1* nuclear speckles per nucleus. To ensure consistency in intensity measurements within and between datasets, standardized imaging and analysis parameters were maintained throughout the project.

Three tumor and three to five normal stromal tissue regions of interest were quantified for each slide using Imaris, cumulatively amounting to ∼600 cell nuclei per slide for tumor and stroma each. For each time point or biopsy block, 2 sections 40 μm apart were used for smRNA-FISH and image analysis, thus adding up to ∼1,200 cell nuclei per biopsy sample for tumor and stromal regions each. The overall *MALAT1* fluorescence intensity data for each cell nucleus (DAPI marked as cell ID) and individual time points from the Imaris output were collated in excel. The violin plots were then generated in R using the ggplot2 and tidyverse packages.[40–42] The output of intensity of each speckle with the corresponding cell ID was transformed into speckle counts/cell nucleus using the dplyr package in R and plotted using ggplot2.[41,43]

Histology

H&E staining was performed at the CSHL Histology Core Facility. Paraffin blocks were sectioned at 5 μm and mounted onto positively charged slides (Fisherbrand Superfrost Plus microscope slides). For H&E staining, slides were processed on a Leica Multistainer (ST5020). Briefly, slides were deparaffinized, rehydrated, and stained

with hematoxylin (Hematoxylin 560 MX, Leica) for 1 min. This was followed by destaining in Define MX-aq (Leica) for 30 s, bluing in Blue Buffer 8 (Leica) for 1 min, and counterstaining with eosin (EOSIN 515 LT, Leica) for 30 s. After dehydration, coverslips were applied to glass slides using a Leica CV5030 robotic coverslipper.

DATA AND CODE AVAILABILITY

All relevant data needed to determine the conclusions stated within the manuscript are available in the main text or the supplemental information. Other raw data/materials used in this study are available upon request to the corresponding author.

ACKNOWLEDGMENTS

The authors thank the patient's family for consenting the donation of the leftover tissue blocks and corresponding pathology reports from AmeriPath to our laboratory for research and for providing additional details of the treatment timeline. We acknowledge the CSHL Cancer Center Microscopy and Histology Shared Resources for services and technical expertise (NCI 2P3OCA45508). The acquisition of the Zeiss LSM 980 confocal microscope with Airyscan2 was funded by NIH 1S10OD034372. This research was supported by NCI 5P01CA013106-Project 3 (D.L.S.) and CSHL/Northwell Health. Written informed consent was obtained from a family member for access to the patient's leftover tissue blocks. The Cold Spring Harbor Laboratory Institutional Review Board (IRB) approved this study (IRB-24-4).

AUTHOR CONTRIBUTIONS

D.A. and S.S. performed the smRNA-FISH. T.-L.W. developed the Airyscan imaging protocol. T.-L.W. and S.S. performed confocal imaging of tumor sections for each tissue block. D.A. and T.-L.W. developed the image analysis pipeline in Imaris and processed images for analysis. S.R. assisted in putting together the patient timeline. D.A. prepared the figures and performed the R analysis. D.A. wrote the manuscript with the assistance of D.L.S. D.L.S. obtained funding for the study. All authors contributed valuable editorial feedback.

DECLARATION OF INTERESTS

D.L.S. is on the Scientific Advisory Board of Amaroq Therapeutics.

SUPPLEMENTAL INFORMATION

Supplemental information can be found online at https://doi.org/10.1016/j.omton.2025.201070.

REFERENCES

1. Kim, J., Harper, A., McCormack, V., Sung, H., Houssami, N., Morgan, E., Mutebi, M., Garvey, G., Soerjomataram, I., and Fidler-Benaoudia, M.M. (2025). Global patterns and trends in breast cancer incidence and mortality across 185 countries. Nat. Med. *31*, 1154–1162. https://doi.org/10.1038/s41591-025-03502-3.
2. Bray, F., Laversanne, M., Sung, H., Ferlay, J., Siegel, R.L., Soerjomataram, I., and Jemal, A. (2024). Global cancer statistics 2022: GLOBOCAN estimates of incidence and mortality worldwide for 36 cancers in 185 countries. CA Cancer J. Clin. *74*, 229–263. https://doi.org/10.3322/CAAC.21834.
3. Burguin, A., Diorio, C., and Durocher, F. (2021). Breast Cancer Treatments: Updates and New Challenges. J. Pers. Med. *11*, 808. https://doi.org/10.3390/JPM11080808.
4. Dittmer, J. (2017). Mechanisms governing metastatic dormancy in breast cancer. Semin. Cancer Biol. *44*, 72–82. https://doi.org/10.1016/J.SEMCANCER.2017.03.006.
5. Elkholi, I.E., Lalonde, A., Park, M., and Côté, J.F. (2022). Breast Cancer Metastatic Dormancy and Relapse: An Enigma of Microenvironment(s). Cancer Res. *82*, 4497–4510. https://doi.org/10.1158/0008-5472.CAN-22-1902/709673/AM/BREAST-CANCER-METASTATIC-DORMANCY-AND-RELAPSE-AN.
6. Fein, M.R., and Egeblad, M. (2013). Caught in the act: Revealing the metastatic process by live imaging. Dis. Model. Mech. *6*, 580–593. https://doi.org/10.1242/DMM.009282/VIDEO-6.
7. Mattick, J.S., Amaral, P.P., Carninci, P., Carpenter, S., Chang, H.Y., Chen, L.L., Chen, R., Dean, C., Dinger, M.E., Fitzgerald, K.A., et al. (2023). Long non-coding RNAs: definitions, functions, challenges and recommendations. Nat. Rev. Mol. Cell Biol. *24*, 430–447. https://doi.org/10.1038/s41580-022-00566-8.
8. Arun, G., Aggarwal, D., and Spector, D.L. (2020). MALAT1 Long Non-Coding RNA: Functional Implications. Noncoding. RNA *6*, 22. https://doi.org/10.3390/ncrna6020022.
9. Ji, P., Diederichs, S., Wang, W., Böing, S., Metzger, R., Schneider, P.M., Tidow, N., Brandt, B., Buerger, H., Bulk, E., et al. (2003). MALAT-1, a novel noncoding RNA, and thymosin β4 predict metastasis and survival in early-stage non-small cell lung cancer. Oncogene *22*, 8031–8041. https://doi.org/10.1038/sj.onc.1206928.
10. Amodio, N., Raimondi, L., Juli, G., Stamato, M.A., Caracciolo, D., Tagliaferri, P., and Tassone, P. (2018). MALAT1: A druggable long non-coding RNA for targeted anti-cancer approaches. J. Hematol. Oncol. *11*, 63. https://doi.org/10.1186/s13045-018-0606-4.
11. Clemson, C.M., Hutchinson, J.N., Sara, S.A., Ensminger, A.W., Fox, A.H., Chess, A., and Lawrence, J.B. (2009). An Architectural Role for a Nuclear Non-coding RNA: NEAT1 RNA is Essential for the Structure of Paraspeckles. Mol. Cell *33*, 717–726. https://doi.org/10.1016/J.MOLCEL.2009.01.026.
12. Hutchinson, J.N., Ensminger, A.W., Clemson, C.M., Lynch, C.R., Lawrence, J.B., and Chess, A. (2007). A screen for nuclear transcripts identifies two linked noncoding RNAs associated with SC35 splicing domains. BMC Genom. *8*, 39. https://doi.org/10.1186/1471-2164-8-39.
13. Tripathi, V., Ellis, J.D., Shen, Z., Song, D.Y., Pan, Q., Watt, A.T., Freier, S.M., Bennett, C.F., Sharma, A., Bubulya, P.A., et al. (2010). The nuclear-retained noncoding RNA MALAT1 regulates alternative splicing by modulating SR splicing factor phosphorylation. Mol. Cell *39*, 925–938. https://doi.org/10.1016/j.molcel.2010.08.011.
14. Huang, N.S., Chi, Y.Y., Xue, J.Y., Liu, M.Y., Huang, S., Mo, M., Zhou, S.L., and Wu, J. (2016). Long non-coding RNA metastasis associated in lung adenocarcinoma transcript 1 (MALAT1) interacts with estrogen receptor and predicted poor survival in breast cancer. Oncotarget *7*, 37957–37965. https://doi.org/10.18632/oncotarget.9364.
15. Shao, J., Zhang, Q., Wang, P., and Wang, Z. (2021). LncRNA MALAT1 promotes breast cancer progression by sponging miR101-3p to mediate mTOR/PKM2 signal transmission. Am. J. Transl. Res. *13*, 10262–10275.
16. Yue, X., Wu, W.Y., Dong, M., and Guo, M. (2021). LncRNA MALAT1 promotes breast cancer progression and doxorubicin resistance via regulating miR-570–3p. Biomed. J. *44*, S296–S304. https://doi.org/10.1016/J.BJ.2020.11.002.
17. Feng, T., Shao, F., Wu, Q., Zhang, X., Xu, D., Qian, K., Xie, Y., Wang, S., Xu, N., Wang, Y., and Qi, C. (2016). miR-124 downregulation leads to breast cancer progression via LncRNA-MALAT1 regulation and CDK4/E2F1 signal activation. Oncotarget *7*, 16205–16216. https://doi.org/10.18632/ONCOTARGET.7578.
18. Jadaliha, M., Zong, X., Malakar, P., Ray, T., Singh, D.K., Freier, S.M., Jensen, T., Prasanth, S.G., Karni, R., Ray, P.S., and Prasanth, K.V. (2016). Functional and prognostic significance of long non-coding RNA MALAT1 as a metastasis driver in ER negative lymph node negative breast cancer. Oncotarget *7*, 40418–40436. https://doi.org/10.18632/oncotarget.9622.
19. Wang, Z., Katsaros, D., Biglia, N., Shen, Y., Fu, Y., Loo, L.W.M., Jia, W., Obata, Y., and Yu, H. (2018). High expression of long non-coding RNA MALAT1 in breast cancer is associated with poor relapse-free survival. Breast Cancer Res. Treat. *171*, 261–271. https://doi.org/10.1007/s10549-018-4839-2.
20. Wang, Y., Zhang, Y., Hu, K., Qiu, J., Hu, Y., Zhou, M., and Zhang, S. (2020). Elevated long noncoding RNA MALAT-1 expression is predictive of poor prognosis in patients with breast cancer: A meta-analysis. Biosci. Rep. *40*, 20200215. https://doi.org/10.1042/BSR20200215/225866.
21. Kumar, D., Gurrapu, S., Wang, Y., Bae, S.Y., Pandey, P.R., Chen, H., Mondal, J., Han, H., Wu, C.J., Karaiskos, S., et al. (2024). LncRNA Malat1 suppresses pyroptosis and T cell-mediated killing of incipient metastatic cells. Nat. Cancer *5*, 262–282. https://doi.org/10.1038/S43018-023-00695-9.
22. Arun, G., and Spector, D.L. (2019). MALAT1 long non-coding RNA and breast cancer. RNA Biol. *16*, 860–863. https://doi.org/10.1080/15476286.2019.1592072.
23. Kwok, Z.H., Roche, V., Chew, X.H., Fadieieva, A., and Tay, Y. (2018). A non-canonical tumor suppressive role for the long non-coding RNA MALAT1 in colon and breast cancers. Int. J. Cancer *143*, 668–678. https://doi.org/10.1002/ijc.31386.

24. Kim, J., Piao, H.-L., Kim, B.-J., Yao, F., Han, Z., Wang, Y., Xiao, Z., Siverly, A.N., Lawhon, S.E., Ton, B.N., et al. (2018). Long noncoding RNA MALAT1 suppresses breast cancer metastasis. Nat. Genet. *50*, 1705–1715. https://doi.org/10.1038/s41588-018-0252-3.

25. Eastlack, S.C., Dong, S., Mo, Y.Y., and Alahari, S.K. (2018). Expression of long noncoding RNA MALAT1 correlates with increased levels of Nischarin and inhibits oncogenic cell functions in breast cancer. PLoS One *13*, e0198945. https://doi.org/10.1371/journal.pone.0198945.

26. Zhang, B., Arun, G., Mao, Y.S., Lazar, Z., Hung, G., Bhattacharjee, G., Xiao, X., Booth, C.J., Wu, J., Zhang, C., and Spector, D.L. (2012). The lncRNA Malat1 is dispensable for mouse development but its transcription plays a cis-regulatory role in the adult. Cell Rep. *2*, 111–123. https://doi.org/10.1016/J.CELREP.2012.06.003.

27. Bhat, A.A., Afzal, O., Afzal, M., Gupta, G., Thapa, R., Ali, H., Hassan almalki, W., Kazmi, I., Alzarea, S.I., Saleem, S., et al. (2024). MALAT1: A key regulator in lung cancer pathogenesis and therapeutic targeting. Pathol. Res. Pract. *253*, 154991. https://doi.org/10.1016/J.PRP.2023.154991.

28. Hussein, M.A., Valinezhad, K., Adel, E., and Munirathinam, G. (2024). MALAT-1 Is a Key Regulator of Epithelial–Mesenchymal Transition in Cancer: A Potential Therapeutic Target for Metastasis. Cancers *16*, 234. https://doi.org/10.3390/CANCERS16010234.

29. Uthman, Y.A., Ibrahim, K.G., Abubakar, B., Bello, M.B., Malami, I., Imam, M.U., Qusty, N., Cruz-Martins, N., Batiha, G.E.S., and Abubakar, M.B. (2021). MALAT1: A Promising Therapeutic Target for the Treatment of Metastatic Colorectal Cancer. Biochem. Pharmacol. *190*, 114657. https://doi.org/10.1016/J.BCP.2021.114657.

30. Zhang, Z., and Lieberman, J. (2024). MALAT1 protects dormant tumor cells from immune elimination. Nat. Cancer *5*, 218–220. https://doi.org/10.1038/s43018-023-00682-0.

31. Adewunmi, O., Shen, Y., Zhang, X.H.F., and Rosen, J.M. (2023). Targeted Inhibition of lncRNA Malat1 Alters the Tumor Immune Microenvironment in Preclinical Syngeneic Mouse Models of Triple-Negative Breast Cancer. Cancer Immunol. Res. *11*, 1462–1479. https://doi.org/10.1158/2326-6066.CIR-23-0045.

32. Meseure, D., Vacher, S., Lallemand, F., Alsibai, K.D., Hatem, R., Chemlali, W., Nicolas, A., De Koning, L., Pasmant, E., Callens, C., et al. (2016). Prognostic value of a newly identified MALAT1 alternatively spliced transcript in breast cancer. Br. J. Cancer *114*, 1395–1404. https://doi.org/10.1038/bjc.2016.123.

33. Dirks, R.M., and Pierce, N.A. (2004). Triggered amplification by hybridization chain reaction. Proc. Natl. Acad. Sci. USA *101*, 15275–15278. https://doi.org/10.1073/PNAS.0407024101.

34. Arun, G., Diermeier, S., Akerman, M., Chang, K.-C., Wilkinson, J.E., Hearn, S., Kim, Y., MacLeod, A.R., Krainer, A.R., Norton, L., et al. (2016). Differentiation of mammary tumors and reduction in metastasis upon Malat1 lncRNA loss. Genes Dev. *30*, 34–51. https://doi.org/10.1101/gad.270959.115.

35. Choi, H.M.T., Schwarzkopf, M., Fornace, M.E., Acharya, A., Artavanis, G., Stegmaier, J., Cunha, A., and Pierce, N.A. (2018). Third-generation *in situ* hybridization chain reaction: Multiplexed, quantitative, sensitive, versatile, robust. Development *145*, dev165753. https://doi.org/10.1242/DEV.165753/48466.

36. Li, J., Cui, Z., Li, H., Lv, X., Gao, M., Yang, Z., Bi, Y., Zhang, Z., Wang, S., Zhou, B., and Yin, Z. (2018). Clinicopathological and prognostic significance of long noncoding RNA MALAT1 in human cancers: A review and meta-analysis. Cancer Cell Int. *18*, 109. https://doi.org/10.1186/s12935-018-0606-z.

37. Martinez-Terroba, E., Plasek-Hegde, L.M., Chiotakakos, I., Li, V., de Miguel, F.J., Robles-Oteiza, C., Tyagi, A., Politi, K., Zamudio, J.R., and Dimitrova, N. (2024). Overexpression of Malat1 drives metastasis through inflammatory reprogramming of the tumor microenvironment. Sci. Immunol. *9*, 5462. https://doi.org/10.1126/sciimmunol.adh5462.

38. Gutschner, T., Hämmerle, M., Eissmann, M., Hsu, J., Kim, Y., Hung, G., Revenko, A., Arun, G., Stentrup, M., Gross, M., et al. (2013). The noncoding RNA MALAT1 is a critical regulator of the metastasis phenotype of lung cancer cells. Cancer Res. *73*, 1180–1189. https://doi.org/10.1158/0008-5472.CAN-12-2850.

39. Shaath, H., Vishnubalaji, R., Elango, R., Khattak, S., and Alajez, N.M. (2021). Single-cell long noncoding RNA (lncRNA) transcriptome implicates MALAT1 in triple-negative breast cancer (TNBC) resistance to neoadjuvant chemotherapy. Cell Death Discov. *7*, 23. https://doi.org/10.1038/s41420-020-00383-y.

40. R Core Team (2024). R: A Language and Environment for Statistical Computing (R Foundation for Statistical Computing).

41. Wickham, H. (2016). ggplot2: Elegant Graphics for Data Analysis (Springer-Verlag).

42. Zhu, A., Ibrahim, J.G., and Love, M.I. (2019). Heavy-tailed prior distributions for sequence count data: removing the noise and preserving large differences. Bioinformatics *35*, 2084–2092. https://doi.org/10.1093/BIOINFORMATICS/BTY895.

43. Wickham, H., François, R., Henry, L., Müller, K., and Vaughan, D. (2023). dplyr: A Grammar of Data Manipulation. https://github.com/tidyverse/dplyr.